Zinc depletion induces ribosome hibernation in mycobacteria

Yunlong Li[a,1], Manjuli R. Sharma[b,1], Ravi K. Koripella[b], Yong Yang[a], Prem S. Kaushal[b,2], Qishan Lin[c], Joseph T. Wade[a,d], Todd A. Gray[a,d], Keith M. Derbyshire[a,d], Rajendra K. Agrawal[b,d,3], and Anil K. Ojha[a,d,3]

[a]Division of Genetics, Wadsworth Center, New York State Department of Health, Albany, NY 12208; [b]Division of Translational Medicine, Wadsworth Center, New York State Department of Health, Albany, NY 12201; [c]Proteomics/Mass Spectrometry Facility, Center for Functional Genomics, University at Albany, Rensselaer, NY 12144; and [d]Department of Biomedical Sciences, University at Albany, Albany, NY 12208

Bacteria respond to zinc starvation by replacing ribosomal proteins that have the zinc-binding CXXC motif (C+) with their zinc-free (C−) paralogues. Consequences of this process beyond zinc homeostasis are unknown. Here, we show that the C− ribosome in *Mycobacterium smegmatis* is the exclusive target of a bacterial protein Y homolog, referred to as mycobacterial-specific protein Y (MPY), which binds to the decoding region of the 30S subunit, thereby inactivating the ribosome. MPY binding is dependent on another mycobacterial protein, MPY recruitment factor (MRF), which is induced on zinc depletion, and interacts with C− ribosomes. MPY binding confers structural stability to C− ribosomes, promoting survival of growth-arrested cells under zinc-limiting conditions. Binding of MPY also has direct influence on the dynamics of aminoglycoside-binding pockets of the C− ribosome to inhibit binding of these antibiotics. Together, our data suggest that zinc limitation leads to ribosome hibernation and aminoglycoside resistance in mycobacteria. Furthermore, our observation of the expression of the proteins of C− ribosomes in *Mycobacterium tuberculosis* in a mouse model of infection suggests that ribosome hibernation could be relevant in our understanding of persistence and drug tolerance of the pathogen encountered during chemotherapy of TB.

C− ribosome | antibiotics | cryo-EM | MPY | MRF

A majority of sequenced bacterial genomes encode paralogues of ribosomal proteins (r-proteins) (1). Among the most conserved r-protein paralogues are the pairs that differ with respect to the zinc-binding CXXC motif (1–3). Proteins with the motif (C+) are incorporated into ribosomes during growth under zinc-rich conditions but are replaced by their zinc-free paralogues (C−) under poor zinc conditions (4–8). C+/− paralogue pairs for S14, S18, L28, and L33 are conserved in the genomes of all mycobacteria (1); nontuberculous and rapid-growing mycobacteria, including *Mycobacterium smegmatis*, also encode a C− paralogue for L31 (1, 9). In the presence of zinc, the zinc uptake regulator, ZurB, binds an upstream *zur-box* to transcriptionally repress the expression of C− paralogues. In low-zinc conditions, ZurB dissociates from the *zur-box*, derepressing transcription (5–7, 10) (*SI Appendix*, Fig. S1A). The coexpression of C− paralogues implies a concerted replacement of all C+ counterparts under zinc-limiting conditions. Each paralogue pair substantially differs in sequence identity (~30–50%) and length, suggesting that their replacements may alter the structure, function, or sensitivity of the ribosome to antibiotics.

In this study, we address the consequence of C+/− substitution on the structural and physiological properties of ribosomes in mycobacteria. We found that a mycobacterial-specific protein Y (MPY) homolog binds exclusively to ribosomes with C− r-proteins. Binding of MPY is dependent on another mycobacterial protein referred to as MPY recruitment factor (MRF), which is coordinately derepressed by ZurB, along with the C− r-proteins paralogues. Binding of MPY increases the stability of the C− 70S ribosome and reduces the binding of kanamycin and streptomycin, thereby protecting the cells from the effects of these antibiotics in zinc-starved conditions. We further show the

expression of C− ribosomal paralogues during infection of *Mycobacterium tuberculosis*, suggesting that ribosome hibernation and associated drug tolerance occur in vivo.

Results

Ribosome Remodeling and Zinc Homeostasis in Mycobacteria. We first established the protein composition of 70S complexes from either high- (supplemented with 1 mM ZnSO$_4$) or low-zinc cultures of *M. smegmatis*. Low zinc in the medium was achieved using a zinc-specific chelator *N,N,N′,N′*-tetrakis(2-pyridylmethyl)-ethylenediamine (TPEN) (*SI Appendix*, Fig. S1B). Analysis by isobaric tags for relative and absolute quantitation mass spectrometry revealed that the relative abundance of all five C− proteins increased by ~20-to 60-fold in 70S ribosomes from low-zinc cultures compared with the ribosomes isolated from high-zinc cultures (*SI Appendix*, Fig. S1 *C and D*). Levels of C+ r-proteins

Significance

Mycobacteria as well as other bacteria remodel their ribosomes in response to zinc depletion by replacing zinc-binding ribosomal proteins with zinc-free paralogues, releasing zinc for other metabolic processes. In this study, we show that the remodeled ribosome acquires a structurally stable but functionally inactive and aminoglycoside-resistant state in zinc-starved *Mycobacterium smegmatis*. Conversely, *M. smegmatis* cells that are growth arrested in zinc-rich conditions have unstable ribosomes and reduced survival. We further provide evidence for ribosome remodeling in *Mycobacterium tuberculosis* in host tissues, suggesting that ribosome hibernation occurs during TB infections. Our findings could offer insights into mechanisms of persistence and antibiotic tolerance of mycobacterial infections.

were concomitantly decreased in low-zinc cultures (*SI Appendix*, Fig. S1 *C* and *D*). We, therefore, refer to 70S complexes from high- and low-zinc cultures as C+ and C− ribosomes, respectively. Consistent with the C+/− substitutions, deletion of the operon encoding C− r-proteins caused growth retardation in both *M. smegmatis* (Δ*msm*$_{c-}$) and *M. tuberculosis* (Δ*mtb*$_{c-}$) mutants in zinc-limiting medium (*SI Appendix*, Fig. S1 *E* and *F*).

Structure Reveals Binding of MPY to C− Ribosomes. To gain insight into differences between C+ and C− ribosomes, we determined the cryo-EM structure of C+ and C− ribosomes from *M. smegmatis*. Our 3.5-Å-resolution structure of the C− ribosome (Fig. 1 *A* and *B* and *SI Appendix*, Fig. S2) further validated its composition by the presence of the densities corresponding to extensions and insertions in S14$_{C-}$, L28$_{C-}$, and L31$_{C-}$ in the cryo-EM map that were absent in their counterparts in the C+ ribosome (Fig. 1*C*). During the final stage of our work, a 3.3-Å-resolution cryo-EM structure of the C+ ribosome was published (11), which matched closely with our C+ ribosome structure and facilitated a high-resolution structural comparison with the C− ribosome. Notably, the C− ribosomes contained the two mycobacterial r-proteins, bS22 and bL37 (Fig. 1*D*), recently described in C+ ribosomes (11–13).

Strikingly, the structure revealed binding of a protein, MSMEG_1878, to C− ribosomes (Fig. 1 *A* and *D* and *SI Appendix*, Fig. S3), which was not observed in either the published (11–13) or our C+ ribosome structures. Because MSMEG_1878 shows structural homology to the *Escherichia coli* stress response

protein Y (pY), featuring a double-stranded RNA-binding domain scaffold with a βαββαα topology (14, 15), we named it MPY. The N-terminal half of MPY binds in the neck region of the 30S ribosomal subunit, encompassing the decoding region and making contacts with the 16S rRNA helices h18 (shoulder), h24 (platform), h44 (body), h31 and h34 (head), and h28 (neck) of the 30S subunit (Fig. 2). It also makes close contacts with 30S head proteins S3 and S9. The binding position of the N-terminal half of MPY overlaps with the binding region of other pY homologs, including ribosome-binding factor A (16), hibernation promotion factor (Hpf), stationary-phase protein (YfiA) (17), and the plastid-specific ribosomal protein 1 (or chloroplast pY) (18, 19). The C-terminal half of MPY, which was partially disordered in our cryo-EM map, runs into the cleft region between the platform and head of the 30S subunit (*SI Appendix*, Fig. S3*C*). Unlike the C+ ribosome, which was present in both rotated and unrotated states, the C− ribosome was almost exclusively found in the unrotated state. Binding of MPY at the decoding region of the C− ribosome likely locks the C− ribosome in its unrotated state, similar to the effect of pY binding to the chloroplast ribosome (19).

Binding of MPY to the C− Ribosome Is Dependent on MRF. MPY expression in cells is constitutive and nonresponsive to zinc (*SI Appendix*, Fig. S4). To verify the specific binding of MPY to C− ribosomes in zinc-starved mycobacteria, we expressed plasmid-borne MPY-FLAG from the *hsp60* promoter in a Δ*mpy* mutant of *M. smegmatis*. We analyzed the association of MPY-FLAG with 70S ribosomes purified from stationary-phase cultures

Fig. 1. A 3.5-Å-resolution cryo-EM structure of the *M. smegmatis* C− 70S ribosome and its interaction with the MPY protein. (*A* and *B*) The 70S cryo-EM structure with two ribosomal subunits in a side-by-side view (*A*) and in the 30S solvent-side view (*B*) is shown. Densities for C− proteins are highlighted in both the small 30S (yellow) and large 50S (blue) subunits. Density for the MPY protein is shown in red. Landmarks of the 30S subunit are body (b), head (h), platform (pt), and shoulder (sh). Landmarks of the 50S subunit are central protuberance (CP), mycobacteria-specific extension in 23S rRNA helix 54 (H54a), protein L1 stalk (L1), and L11 stalk base (Sb). The arrow in *B* points to the mRNA entrance channel. (*C*) Modeling of all five C− r-proteins into their corresponding cryo-EM densities. The extensions and insertions specific to C− r-proteins S14$_{C-}$, L28$_{C-}$, and L31$_{C-}$ are depicted in red. Regions of the cryo-EM densities corresponding to relatively less resolved C− r-proteins in peripheral regions of the ribosome are shown as C-α atoms. (*D*) Representative segments of the cryo-EM map with modeled rRNA and proteins from both ribosomal subunits: 16S rRNA helix 44 (h44), 30S protein S22 (S22), MPY, 23S rRNA helix 36 (H36), and 50S protein L37 (L37).
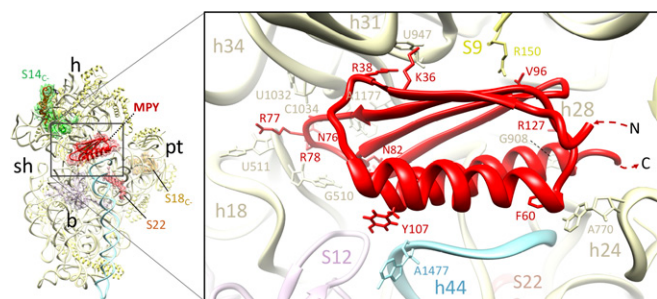
Fig. 2. Molecular interactions of MPY (red) with the 30S subunit components. The 16S rRNA helix 44 (blue) and proteins S9 (yellow) and S12 (pink) are highlighted, whereas the remainder of the 16S rRNA segment is shown in pale yellow. Numbers after head (h) identify the 16S rRNA helix. Numbering on all interacting nucleotide and amino acid residues is color coded. N and C after dashed red arrows indicate disordered regions on both of the termini of MPY that could not be modeled (*SI Appendix*, Fig. S3). The thumbnail depicts the overall orientation of the 30S subunit. b, Body; pt, platform; sh, shoulder.

grown in either high- or low-zinc medium. Consistent with the constitutive expression of native MPY (*SI Appendix*, Fig. S4), total cellular abundance of MPY-FLAG was similar regardless of zinc availability (Fig. 3A). However, MPY-FLAG was predominantly associated with the 70S ribosome only in low-zinc cultures (Fig. 3A). We next asked if incorporation of C− r-proteins in ribosomes is sufficient to induce MPY binding. We engineered a plasmid with mutations in the *zur-box* upstream of the msm_{c-} promoter $P^{zur-box}$ (*SI Appendix*, Fig. S1A) to constitutively produce C− r-proteins, independent of zinc availability in the medium (*SI Appendix*, Fig. S5 A and B) (20). This constitutive promoter (P^{const}) was not repressed by zinc supplementation (*SI Appendix*, Fig. S5C) and produced 70S ribosomes with 20- to 60-fold higher levels of C− r-proteins relative to the ZurB repressed wild-type $P^{zur-box}$ (*SI Appendix*, Fig. S5D). We then deleted chromosomal *mpy* in the P^{const}-msm_{c-} strain and expressed plasmid-borne MPY-FLAG from the *hsp60* promoter to analyze the association of MPY-FLAG with 70S ribosomes from high- and low-zinc cultures. As expected, the 70S ribosomes from both cultures had C− r-proteins, but MPY-FLAG association was approximately threefold higher in low-zinc cells than in high-zinc cells (Fig. 3B). We also noticed higher MPY association with C− ribosomes produced by the P^{const}-msm_{c-} strain than with C+ ribosomes produced by wild-type cells, both grown in zinc-rich medium (Fig. 3B). Thus, efficient binding of MPY to the ribosome requires both C− r-protein expression and zinc depletion.

Individual deletion of neither S14$_{C-}$ nor S18$_{C-}$ altered MPY binding to the modified ribosome (*SI Appendix*, Fig. S6), suggesting that another zinc-responsive factor facilitates MPY association with the 30S subunit of the C− ribosome. We hypothesized MSMEG_6069 as a possible candidate given its coexpression as a gene in the *c-* operon in *M. smegmatis* genome (*SI Appendix*, Fig. S1A) and the ZurB-dependent regulation of its homolog (Rv0106) in *M. tuberculosis* (6). Moreover, we observed a poorly resolved additional mass of protein density located between the head and platform on the solvent side of the 30S subunit of the C− ribosome. This additional density is visible at significantly lower threshold values, and its overall size is consistent with MSMEG_6069. FLAG-tagged MSMEG_6069, driven by its own promoter complementing an *M. smegmatis* strain carrying in-frame deletion of the chromosomal gene, confirmed its expression and binding to the ribosome under low-zinc conditions (Fig. 3C). To test whether MSMEG_6069 facilitates MPY binding to the C− ribosome, we expressed MPY-FLAG in a mutant strain with chromosomal deletions of MSMEG_6069 (in frame) and *mpy* and analyzed the association of MPY-FLAG with 70S ribosomes purified from cells grown in low-zinc medium. MPY binding to C− ribosomes was diminished

in Δ*MSMEG_6069* mutant (Fig. 3D). We renamed MSMEG_6069 as MRF. Despite a constitutive expression of MRF with the other C− r-proteins in the P^{const}-msm_{c-} strain, efficient binding of MPY required zinc depletion (Fig. 3B). We, therefore, conclude that expression of MRF is necessary but not sufficient for saturated occupancy of MPY. MPY occupancy likely peaks during downregulation of protein synthesis in zinc-depleted cells, as its binding would compete directly with mRNA, tRNA, and initiation and elongation factors (*SI Appendix*, Fig. S7).

MPY Is Required for Stability of 70S Ribosomes in Growth-Arrested Mycobacteria. The established role of MPY homologs in ribosome preservation in other organisms (15–18, 21, 22) led us to inquire if MPY-bound C− ribosomes are more stable in mycobacteria that are growth arrested under zinc starvation relative to their C+ counterparts in cells that are growth arrested in zinc-rich conditions. Ribosome degradation was measured as the fraction of acid-soluble radioactivity released from the degradation of ^{3}H-uridine–labeled total cellular RNA (23). Degradation during growth arrest was compared between cells harboring MPY-bound C− ribosomes from low-zinc cultures and those with C+ ribosomes from high-zinc cultures. Complete growth arrest was achieved by resuspending the stationary-phase cells in PBS with either low or high levels of zinc. To determine the specific contribution of MPY, a low-zinc culture of a Δ*mpy* mutant harboring C− ribosomes was also included. Degradation of C− ribosomes was significantly slower than both C+ and MPY-free C− ribosomes during 4 d of starvation (Fig. 4A), implying that C+ ribosomes are intrinsically less stable than their C− counterparts. Furthermore, the stability of the C− ribosome is MPY dependent (Fig. 4A). To obtain further insight into MPY-dependent stabilization of C− ribosomes, we compared the relative abundance of the 70S ribosome and the 50S and 30S subunits in *M. smegmatis* cells maintained in PBS with either high or low zinc for 2 d. Ribosomes from actively growing culture from
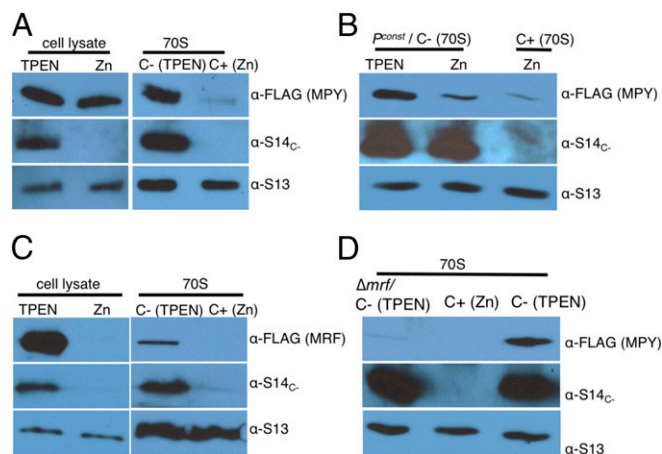

Fig. 3. MRF-dependent exclusive binding of MPY to C− ribosomes. (*A*) Analysis of FLAG-tagged MPY in total cell lysates and 70S particles from low- and high-zinc cultures of Δ*mpy* mutant of *M. smegmatis* expressing MPY-FLAG. Antibodies against purified recombinant *M. smegmatis* S14$_{C-}$ and *E. coli* S13 were used as controls. (*B*) Analysis of MPY-FLAG in 70S ribosomes from low- and high-zinc cultures of Δ*mpy* strain expressing *c-* operon from the P^{const} and MPY-FLAG from a constitutive promoter (*SI Appendix*, Fig. S5); 70S ribosomes from a high-zinc culture of Δ*mpy* strain with wild-type *c-* operon and expressing MPY-FLAG from the same plasmid were used as control. (*C*) Analysis of MRF (MSMEG_6069)-FLAG in cell lysate and 70S particles from low- and high-zinc cultures of *M. smegmatis*. Chromosomal copy of MRF was deleted in the strain, expressing plasmid-borne MRF-FLAG from the endogenous promoter. (*D*) Analysis of MPY-FLAG in 70S C− ribosomes from low-zinc cultures of Δ*mrf* strain. The strain also had deletion in chromosomal *mpy* while expressing plasmid-borne MPY-FLAG from a constitutive promoter. Purified 70S C+ and C− ribosomes were controls.
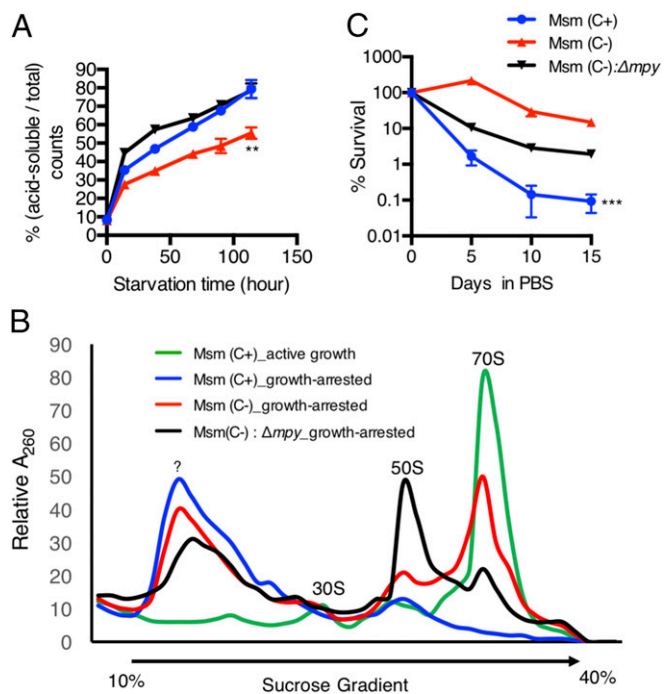
Fig. 4. Structurally stable C− ribosomes support long-term survival of zinc-starved mycobacteria. (A) Comparison of degradation profiles of ribosomes in high-zinc (1 mM ZnSO₄) or low-zinc (1 μM TEPN) cultures of *M. smegmatis* indicated as Msm (C+) and Msm (C−), respectively, and a low-zinc culture of *Δmpy* mutant. Cells were cultured in medium with 1 μCi/mL ³H-uridine until stationary phase, and they were washed and resuspended in PBS with high or low zinc for indicated time periods (*x* axis); radionucleotides released from RNA degradation were measured as percentages of the total counts (*y* axis). (B) Abundance of 70S, 50S, and 30S particles in Msm (C+), Msm (C−), and *Δmpy* mutant of Msm (C−). Cells from high- or low-zinc cultures were washed and incubated in PBS with high or low zinc for 2 d, and ribosomes were purified on a 36 mL 10–40% sucrose gradient. Ribosomes purified from an actively growing high-zinc culture was used as a reference. The symbol ? denotes degradation products of unknown identity. (C) Survival of Msm (C+), Msm (C−), and Msm (C−):*Δmpy* under growth-arrested conditions. Stationary-phase cells from high- or low-zinc cultures were resuspended in high- or low-zinc PBS as used in *B* for indicated times, and viable cells were enumerated on M63 agar with 0.2% glucose. Data in *A* and *C* represent mean ± SE (*n* = 3). **P < 0.01; ***P < 0.001.

high-zinc Sauton's medium were used as reference. As expected, the relative abundance of 70S in all starved cells was lower than the growing cells, with concomitant accumulation of degradation products (Fig. 4*B*). Moreover, the relative abundance of 70S was severely diminished in high-zinc *M. smegmatis* cells compared with cells maintained under low-zinc conditions (Fig. 4*B*). Zinc-depleted cells of *Δmpy* representing MPY-free C− ribosomes had lower levels of 70S particles than those in zinc-depleted wild-type cells, while there was a sharp increase in the abundance of 50S particles (Fig. 4*B*). This implies that MPY is involved in stabilizing the 30S ribosomal subunit without affecting the 50S ribosomal subunit, thereby rendering stable 70S particles. The presence of MPY at the interface of 30S and 50S (Fig. 1*A*) and stabilization of an unrotated 70S conformation are consistent with this model. Loss of cellular viability was consistent with the relative abundance of 70S in *M. smegmatis* cells (Fig. 4*C*). During an extended period of incubation in high- or low-zinc PBS, *M. smegmatis* cells harboring C− ribosomes (in low-zinc PBS) were >100-fold more viable than their counterparts with C+ ribosomes in high-zinc PBS (Fig. 4*C*). Viability loss in *Δmpy* was moderate relative to wild-type cells with C+ ribosomes, corresponding to a relatively moderate loss in the 70S complexes in the mutant (Fig. 4*B*).

MPY Confers Aminoglycoside Resistance in Zinc-Starved Mycobacteria.

Based on the C− ribosome structure, ribosome occupancy by MPY is predicted to directly interfere with the binding of the aminoglycosides kanamycin and streptomycin (Fig. 5 *A* and *B*). Kanamycin binds in the minor groove of the 16S rRNA h44 and flips out the universally conserved bases A1476 and A1477 residues (*E. coli*: A1492 and A1493) from the helix (24) (Fig. 5*A*) to stabilize the minihelix formed between the anticodon of a near-cognate tRNA and mRNA codon. This allows binding and accommodation of ambiguous tRNAs during protein synthesis as described for another aminoglycoside, paromomycin (25). Binding of kanamycin to MPY-bound C− ribosomes would result in a steric clash, as the space necessary for flipping of residue A1477 is
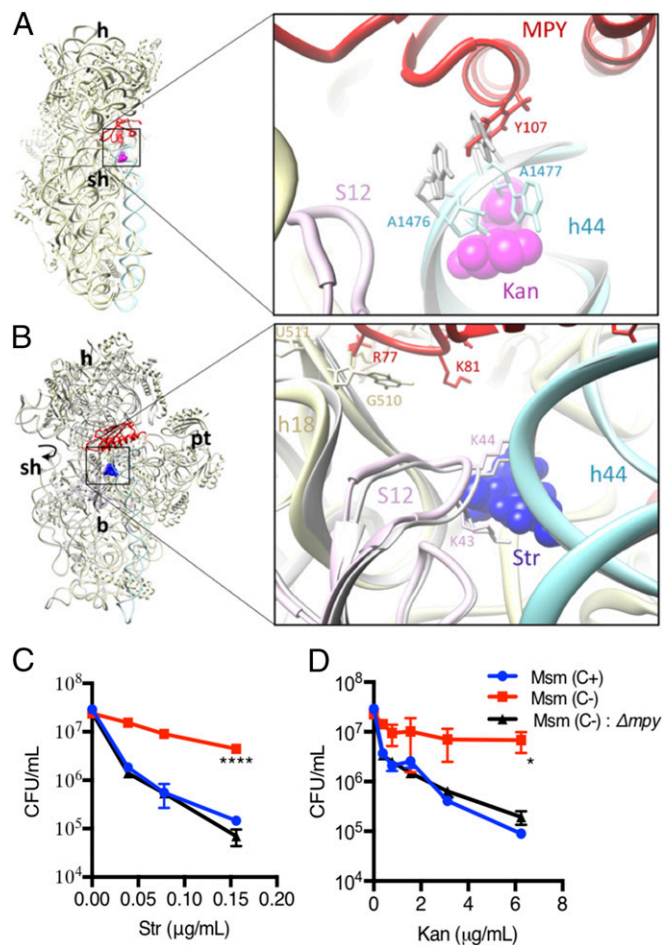

Fig. 5. C− ribosomes are resistant to aminoglycosides in growth-arrested mycobacteria under zinc starvation. (A) Superimposition of the kanamycin (Kan)-bound structure of the 16S rRNA h44 oligonucleotides (25) [Protein Data Bank (PDB) ID code 2ESI] onto the equivalent region of the h44 in the C− ribosome structure. Universally conserved A1477 (light blue) corresponding to A1493 in *E. coli*, which is flipped out on Kan (magenta) binding to RNA segment (gray), would be in a steric clash with Y107 of MPY. (B) Superimposition of the 30S structures of C+ (11) (gray; PDB ID code 5O61) and our C− ribosomes, showing opening of the binding pocket of streptomycin (Str) in C− ribosome by ~3 Å due to an outward rotation of the 30S shoulder (depicted by a curved arrow in *Left*). All landmarks of the ribosome are labeled as introduced in Fig. 1. b, Body; h, head; pt, platform; sh, shoulder. (C and D) Effect of *mpy* deletion on sensitivity of C− ribosomes to Str (C) and Kan (D). High-zinc (1 mM ZnSO₄) or low-zinc (1 μM TEPN) stationary-phase cells, indicated as Msm (C+) or Msm (C−), respectively, of wild-type or *Δmpy* were resuspended in high- or low-zinc PBS with indicated concentrations of antibiotics for 2 d before enumerating the viable cells. Data in *C* and *D* represent mean ± SE (*n* = 3). *P < 0.05; ****P < 0.0001.

occupied by a highly conserved amino acid residue (Y107) of MPY (Fig. 5A). Streptomycin binds in the cavity formed between the r-protein S12 and 16S rRNA helices h1, h18, h27, and h44, making a direct interaction with the K44 (K45 in *E. coli*) residue of S12 (Fig. 5B) (26). In the presence of MPY, the shoulder region, which includes h18 and protein S12 (11), rotates outward. This outward movement opens up the streptomycin-binding pocket by ~3 Å, which would likely alter the binding affinity of streptomycin. Exposure to streptomycin and kanamycin decreased viability of growth-arrested Δ*mpy* cells harboring C− ribosomes to the level observed for cells with C+ ribosomes (Fig. 5 *C* and *D*). The contribution of MPY to drug tolerance is likely a combination of both increased stability of ribosomes and decreased accessibility to the aminoglycosides. Since the MPY-bound ribosome would also be sterically precluded from binding of canonical ligands, like mRNA, tRNAs, or other translational factors (*SI Appendix*, Fig. S7), the mechanistic aspects of MPY-dependent antibiotic resistance are only applicable to idle 70S ribosomes in growth-arrested cells. Thus, MPY plays a crucial role in maintaining an antibiotic-resistant pool of structurally stable C− ribosomes in mycobacterial cells that are growth arrested under zinc-limiting conditions. Subsequent removal of MPY by competition with abundant translation factors (27) could facilitate rapid recovery of normal protein synthesis during outgrowth.

Expression of C− Ribosomes in *M. tuberculosis* During Infection.
Finally, we asked if C− ribosomes are expressed in *M. tuberculosis* in lungs of infected mice. We determined the in vivo expression of the mtb_{c-} operon by using a strain of *M. tuberculosis* carrying a transcriptional fusion of Dendra2 to the mtb_{c-} promoter as a reporter of induction (*SI Appendix*, Fig. S8). In C57BL/6 mice, ~12% of the bacilli expressed the reporter after 4 wk of infection, increasing to ~40% after 14 wk of infection (Fig. 6). Interestingly, inclusion of 10 mM ZnSO$_4$ in the drinking water of the animals limited the expression of the reporter at 14 wk of infection to ~20% of the bacilli (Fig. 6). The gross bacterial burden did not respond to zinc treatment (*SI Appendix*, Fig. S9A), suggesting that bacilli expressing either of the two types of ribosomes are viable in their respective host environments.

The increase in the reporter expression from the acute (4 wk) to the chronic phase of infection (14 wk) can be reasonably explained from the known differential host responses with respect to zinc availability during acute and chronic phases of infection. During the acute phase (<4 wk) of infection, the zinc concentration in the phagosomal compartments of infected macrophages is increased by ~15-fold (28, 29). However, zinc is likely chelated to a low level by neutrophil-secreted calprotectin in the necrotizing center of TB lesions, which develop after activation of adaptive immunity during the chronic phase (>4 wk) (30). We reasoned that a mouse model producing more necrotic lesions on *M. tuberculosis* infection would further induce the expression of the mtb_{c-} operon. In support of this model, almost saturating levels of Dendra2-positive bacilli were observed in the lungs of the susceptible mouse strain, C3HeB/FeJ (Kramnick) (*SI Appendix*, Fig. S9 *B* and *C*), which develops significantly more necrotizing lesions than C57BL/6 mice (31).

Discussion
Mycobacterial ribosomes are reprogrammed during zinc starvation to replace multiple r-proteins that contain the zinc-binding CXXC motif (C+) with C− paralogues. Here, we describe the consequences of the C− r-protein replacements on the structural and functional properties of the ribosome. The structural analysis identifies the C− ribosome in an inactive state, in which its decoding region is occupied by a mycobacterial pY homolog, MPY. MPY is a constitutively expressed protein, but its recruitment to the ribosome requires induction of MRF expression that occurs only under zinc limitations. The C+ ribosome, therefore, remains inaccessible to MPY, raising questions about the conditions promoting hibernation of this ribosome. Such
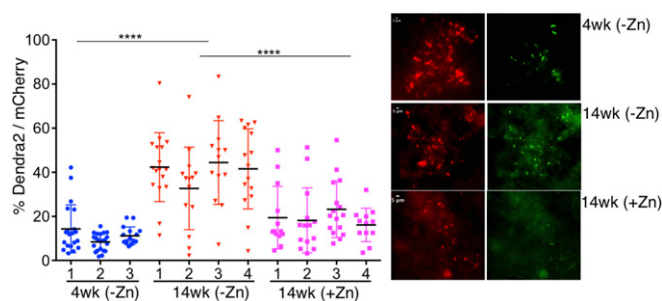

Fig. 6. Expression of C− ribosomes in *M. tuberculosis* during growth in mouse lungs. Percentage of the *M. tuberculosis* (Erdman) subpopulation expressing Dendra2 (green) from the mtb_{c-} promoter relative to the entire population constitutively expressing mCherry (red) from the *hsp60* promoter at 4 and 14 wk postinfection in lungs of C57BL/6 mice. The effect of dietary zinc supplement on expression of Dendra2 at 14 wk of infection is also included. The number on the *x* axis denotes an individual mouse in each group. Each data point on the *y* axis represents a view field with at least 15 red bacilli. Representative micrographs from each group are shown in *Right*. Each data point corresponds to one mouse. Bacterial burdens in the analyzed lungs are provided in *SI Appendix*, Fig. S9. ****$P < 0.0001$ (Mann–Whitney *U*).

possibility is further diminished by instability of the C+ ribosome in growth-arrested cells.

Recruitment of MRF and MPY preserves the 70S C− ribosome in a structurally stable and aminoglycoside-resistant state. Thus, growth-arrested cells harboring these ribosomes not only persist longer but also, remain recalcitrant to aminoglycosides. Moreover, cells harboring saturating levels of hibernating ribosome likely represent a physiological state with minimal levels of translation activity, presumably leading to metabolic slowdown. A detailed comparison of metabolic states of zinc-starved cells with those exposed to other growth-arresting conditions, such as hypoxia and macronutrient starvation, is likely to yield molecular signatures of dormancy in mycobacteria.

Mycobacterial C− ribosomes are similar to *E. coli* ribosomes, which constitutively utilize C− forms of S14, S18, L28, and L33, and are targeted by either YfiA or the ribosome modulation factor (Rmf) and Hpf during stationary-phase growth (32). Binding of YfiA and Hpf is mutually exclusive and results in stabilization of ribosomes as either 70S or 100S particles, respectively. Although the physiological significance of ribosome hibernation in two distinct physical states (70S and 100S) is unknown, the mechanism leading to formation of one state at the expense of the other is elucidated through the structure of the ribosome in complex with each of the three proteins (17). On binding to the ribosome, the extended C-terminal region of YfiA sterically inhibits binding by Rmf. In the absence of YfiA, Rmf binding results in the formation of a 90S complex, to which Hpf binds and forms the stable 100S complex. The requirement of MRF for MPY binding parallels the Hpf–Rmf interaction, although MPY shares the property of YfiA in terms of having the extended C terminus. In fact, MPY function more closely mimics YfiA, as it stabilizes a monomer 70S state. The multiple approaches to generating hibernating ribosomes is further underscored by the fact that *Staphylococcus aureus* and *Bacillus subtilis*, which do not encode either YfiA or Rmf homologs, utilize Hpf with an extended C terminus to produce 100S particles (33–35). The structural basis of the MPY–MRF interaction will further clarify the individual roles of the two proteins in ribosome stability, specifically the 30S subunit. It is noteworthy that MPY has insignificant influence on the stability of the 50S subunit in growth-arrested mycobacteria (Fig. 4*B*), suggesting that other factors are involved in stabilization of the large subunit under zinc-limiting conditions. One possibility is that one or all of the C− r-protein paralogues contribute to intrinsic stabilization of the 50S subunit.

The high conservation of both MPY and MRF homologs across mycobacteria combined with the coregulation of MRF and C− r-proteins by ZurB in both *M. smegmatis* and *M. tuberculosis* is consistent with their cofunction in ribosome hibernation in *M. tuberculosis*. MPY-dependent ribosome hibernation during the chronic phase of *M. tuberculosis* infection is also suggested by activation of the promoter driving the C− r- protein expression. Future experiments to determine the level of MPY occupancy on the C− ribosome in vivo and their tolerance to antibiotics will address the contribution of ribosome hibernation in development of drug-tolerant *M. tuberculosis* persisters, which are considered an impediment to effective treatments for TB. The chronic phase of infection in C57BL/6 mice is associated with a significant slowdown in bacterial replication rate (36). Although factors contributing to slow replication during chronic infection remain unclear, metabolic slowdown from zinc depletion-induced ribosome hibernation is a possible cause of this reduced growth and is consistent with the elevated expression of C− r-proteins at this phase of infection (Fig. 6). The only known mechanism of in vivo drug tolerance in *M. tuberculosis* involves an efflux pump (37), which is active in replicating bacilli in macrophages. The formation of C− ribosomes in vivo may also enhance drug tolerance, although this hypothesis remains untested. If this was shown, the C− ribosome would provide an effective drug target for preventing long-term persistence of *M. tuberculosis*.

The addition of zinc to the diet of mice suppressed C− r-protein expression and probably offers a route to alter *M. tuberculosis* survival in vivo. However, the benefits of zinc in TB therapy are not obvious (38). Moreover, achieving the desirable concentration of zinc specifically in TB lesions would represent a significant challenge. A more direct pharmacological approach would be to prevent assembly of the C− ribosome and/or its interaction with MPY and MRF.

In conclusion, we have identified a unique mechanism of ribosome hibernation used by mycobacteria under zinc starvation. Further insights into molecular interactions and interplay among MPY, MRF, and the ribosome could potentially lead to an effective treatment of mycobacterial infections.

Materials and Methods

Referenced details of the materials and methods, including plasmids (*SI Appendix*, Table S1), bacterial strains (*SI Appendix*, Table S1), and oligonucleotides (*SI Appendix*, Table S2), are provided in *SI Appendix*. All animal experiments were approved by the Institutional Animal Care and Use Committee (IACUC) of the Wadsworth Center. Statistics of cryo-EM image processing and molecular modeling are provided in *SI Appendix*, Table S3.

1. Yutin N, Puigbò P, Koonin EV, Wolf YI (2012) Phylogenomics of prokaryotic ribosomal proteins. *PLoS One* 7:e36972.
2. Makarova KS, Ponomarev VA, Koonin EV (2001) Two C or not two C: Recurrent disruption of Zn-ribbons, gene duplication, lineage-specific gene loss, and horizontal gene transfer in evolution of bacterial ribosomal proteins. *Genome Biol* 2:RESEARCH 0033.
3. Panina EM, Mironov AA, Gelfand MS (2003) Comparative genomics of bacterial zinc regulons: Enhanced ion transport, pathogenesis, and rearrangement of ribosomal proteins. *Proc Natl Acad Sci USA* 100:9912–9917.
4. Nanamiya H, et al. (2004) Zinc is a key factor in controlling alternation of two types of L31 protein in the Bacillus subtilis ribosome. *Mol Microbiol* 52:273–283.
5. Gabriel SE, Helmann JD (2009) Contributions of Zur-controlled ribosomal proteins to growth under zinc starvation conditions. *J Bacteriol* 191:6116–6122.
6. Maciag A, et al. (2007) Global analysis of the Mycobacterium tuberculosis Zur (FurB) regulon. *J Bacteriol* 189:730–740.
7. Owen GA, Pascoe B, Kallifidas D, Paget MS (2007) Zinc-responsive regulation of alternative ribosomal protein genes in Streptomyces coelicolor involves zur and sigmaR. *J Bacteriol* 189:4078–4086.
8. Hensley MP, et al. (2012) Characterization of Zn(II)-responsive ribosomal proteins YkgM and L31 in E. coli. *J Inorg Biochem* 111:164–172.
9. Ojha A, Hatfull GF (2007) The role of iron in *Mycobacterium smegmatis* biofilm formation: The exochelin siderophore is essential in limiting iron conditions for biofilm formation but not for planktonic growth. *Mol Microbiol* 66:468–483.
10. Prisic S, et al. (2015) Zinc regulates a switch between primary and alternative S18 ribosomal proteins in Mycobacterium tuberculosis. *Mol Microbiol* 97:263–280.
11. Hentschel J, et al. (2017) The complete structure of the Mycobacterium smegmatis 70S ribosome. *Cell Reports* 20:149–160.
12. Li Z, et al. (2018) Cryo-EM structure of Mycobacterium smegmatis ribosome reveals two unidentified ribosomal proteins close to the functional centers. *Protein Cell* 9: 384–388.
13. Yang K, et al. (2017) Structural insights into species-specific features of the ribosome from the human pathogen Mycobacterium tuberculosis. *Nucleic Acids Res* 45: 10884–10894.
14. Ye K, Serganov A, Hu W, Garber M, Patel DJ (2002) Ribosome-associated factor Y adopts a fold resembling a double-stranded RNA binding domain scaffold. *Eur J Biochem* 269:5182–5191.
15. Vila-Sanjurjo A, Schuwirth BS, Hau CW, Cate JH (2004) Structural basis for the control of translation initiation during stress. *Nat Struct Mol Biol* 11:1054–1059.
16. Datta PP, et al. (2007) Structural aspects of RbfA action during small ribosomal subunit assembly. *Mol Cell* 28:434–445.
17. Polikanov YS, Blaha GM, Steitz TA (2012) How hibernation factors RMF, HPF, and YfiA turn off protein synthesis. *Science* 336:915–918.
18. Sharma MR, et al. (2007) Cryo-EM study of the spinach chloroplast ribosome reveals the structural and functional roles of plastid-specific ribosomal proteins. *Proc Natl Acad Sci USA* 104:19315–19320.
19. Bieri P, Leibundgut M, Saurer M, Boehringer D, Ban N (2017) The complete structure of the chloroplast 70S ribosome in complex with translation factor pY. *EMBO J* 36: 475–486.
20. Eckelt E, Jarek M, Frömke C, Meens J, Goethe R (2014) Identification of a lineage specific zinc responsive genomic island in Mycobacterium avium ssp. paratuberculosis. *BMC Genomics* 15:1076.
21. Maki Y, Yoshida H, Wada A (2000) Two proteins, YfiA and YhbH, associated with resting ribosomes in stationary phase Escherichia coli. *Genes Cells* 5:965–974.
22. Akiyama T, et al. (2017) Resuscitation of *Pseudomonas aeruginosa* from dormancy requires hibernation promoting factor (PA4463) for ribosome preservation. *Proc Natl Acad Sci USA* 114:3204–3209.
23. Zundel MA, Basturea GN, Deutscher MP (2009) Initiation of ribosome degradation during starvation in Escherichia coli. *RNA* 15:977–983.
24. François B, et al. (2005) Crystal structures of complexes between aminoglycosides and decoding A site oligonucleotides: Role of the number of rings and positive charges in the specific binding leading to miscoding. *Nucleic Acids Res* 33:5677–5690.
25. Ogle JM, et al. (2001) Recognition of cognate transfer RNA by the 30S ribosomal subunit. *Science* 292:897–902.
26. Carter AP, et al. (2000) Functional insights from the structure of the 30S ribosomal subunit and its interactions with antibiotics. *Nature* 407:340–348.
27. Sharma MR, et al. (2010) PSRP1 is not a ribosomal protein, but a ribosome-binding factor that is recycled by the ribosome-recycling factor (RRF) and elongation factor G (EF-G). *J Biol Chem* 285:4006–4014.
28. Botella H, et al. (2011) Mycobacterial p(1)-type ATPases mediate resistance to zinc poisoning in human macrophages. *Cell Host Microbe* 10:248–259.
29. Wagner D, et al. (2005) Elemental analysis of Mycobacterium avium-, Mycobacterium tuberculosis-, and Mycobacterium smegmatis-containing phagosomes indicates pathogen-induced microenvironments within the host cell's endosomal system. *J Immunol* 174:1491–1500.
30. Corbin BD, et al. (2008) Metal chelation and inhibition of bacterial growth in tissue abscesses. *Science* 319:962–965.
31. Harper J, et al. (2012) Mouse model of necrotic tuberculosis granulomas develops hypoxic lesions. *J Infect Dis* 205:595–602.
32. Ueta M, et al. (2005) Ribosome binding proteins YhbH and YfiA have opposite functions during 100S formation in the stationary phase of Escherichia coli. *Genes Cells* 10:1103–1112.
33. Ueta M, Wada C, Wada A (2010) Formation of 100S ribosomes in Staphylococcus aureus by the hibernation promoting factor homolog SaHPF. *Genes Cells* 15:43–58.
34. Khusainov I, et al. (2017) Structures and dynamics of hibernating ribosomes from *Staphylococcus aureus* mediated by intermolecular interactions of HPF. *EMBO J* 36: 2073–2087.
35. Beckert B, et al. (2017) Structure of the *Bacillus subtilis* hibernating 100S ribosome reveals the basis for 70S dimerization. *EMBO J* 36:2061–2072.
36. Muñoz-Elías EJ, et al. (2005) Replication dynamics of Mycobacterium tuberculosis in chronically infected mice. *Infect Immun* 73:546–551.
37. Adams KN, et al. (2011) Drug tolerance in replicating mycobacteria mediated by a macrophage-induced efflux mechanism. *Cell* 145:39–53.
38. Grobler L, Nagpal S, Sudarsanam TD, Sinclair D (2016) Nutritional supplements for people being treated for active tuberculosis. *Cochrane Database Syst Rev* 6:CD006086.